A Framework for Morphological Feature Extraction of Organs from MR Images for Detection and Classification of Abnormalities

Villarini, B., Asaturyan, H., Thomas, E.L., Mould, R. and Bell, J.D.

https://dx.doi.org/10.1109/CBMS.2017.49

A Framework for Morphological Feature Extraction of Organs from MR Images for Detection and Classification of Abnormalities

Barbara Villarini[1], Hykoush Asaturyan[2]
Computer Science Department
University of Westminster
London, United Kingdom
[1]*b.villarini@westminster.ac.uk*
[2]*h.asaturyan@westminster.ac.uk*

E. Louise Thomas[3], Rhys Mould, Jimmy D. Bell[4]
Centre for Optimal Health, Life Sciences Department
University of Westminster
London, United Kingdom
[3]*l.l.thomas@westminster.ac.uk*
[4]*j.bell@westminster.ac.uk*

***Abstract*—In clinical practice, a misdiagnosis can lead to incorrect or delayed treatment, and in some cases, no treatment at all; consequently, the condition of a patient may worsen to varying degrees, in some cases proving fatal. The accurate 3D reconstruction of organs, which is a pioneering tool of medical image computing (MIC) technology, plays a key role in computer aided diagnosis (CADx), thereby enabling medical professionals to perform enhanced analysis on a region of interest. From here, the shape and structure of the organ coupled with measurements of its volume and curvature can provide significant guidance towards establishing the severity of a disorder or abnormality, consequently supporting improved diagnosis and treatment planning. Moreover, the classification and stratification of organ abnormalities is widely utilised within biomedical, forensic and MIC research for exploring and investigating organ deformations following injury, illness or trauma. This paper presents a tool that calculates, classifies and analyses pancreatic volume and curvature following their 3D reconstruction. Magnetic resonance imaging (MRI) volumes of 115 adult patients are evaluated in order to examine a correlation between these two variables. Such a tool can be utilised in the scope of much greater research and investigation. It can also be incorporated into the development of effective medical image analysis software application in the stratification of subjects and targeting of therapies.**

***Keywords*-computer aided diagnosis (CADx), organ volume, organ curvature, 3D organ reconstruction, magnetic resonance imaging (MRI).**

I. Introduction

The computer aided investigation of organ morphology variations in patients with disorders such as Type 2 diabetes mellitus [1], polycystic liver disease [2], renal disease and obesity [3] has played a significant role in boosting the quality of biomedical research, thus providing a valuable analytical "second opinion" for the medical professional. Computer aided diagnosis (CADx) software is employed in several fields; for example it has been used to calculate accurate volume measurements for fetal echocardiography [4]. Studies have also highlighted a relationship between extensor muscle volume and the magnitude of the sagittal curvature [5]. Similarly, investigation into organ volume and curvature, especially those of abnormalities, have provided patterns of interest to the biomedical researcher. Moreover, the use of 3D reconstruction of medical images is now an integral part of clinical medicine. Recently, reconstruction of CT, MR and ultrasound image datasets into 3D volume has gained wide interest. For example, 3D reconstruction techniques from medical images are used to explore craniocerebral trauma [6], providing an effective approach for forensic investigation in cases of survived craniocerebral trauma patients without direct evidences interpreting original trauma patterns. This could potentially be helpful in exploring further injury. The 3D reconstruction of brachial plexus [7] determines the individual brachial plexus anatomy with maximum detail and accuracy, in view of utilising these methods in a practical clinical setting. The thin slice 3D reconstruction in breast cancer patients demonstrates a better technique for accurate evaluation of breast cancer [8]. The influence of head motion on the accuracy of 3D reconstruction is explored in [9] as patient movement during the imaging process may result in motion artefacts such as blurring and defects, which can appear in medical imaging.

Thus, the enhanced precision of 3D organ reconstruction coupled with morphological feature-based classification may reveal previously unknown correlations between various factors such as volume, curvature, anthropometric, ethnicity and health status. The proposed tool presented in this paper can also be incorporated within a much wider scope of medical imaging analysis software application. The advantages of utilising such a tool in CADx may support the reduction of misdiagnosis rates, thus lowering the probability of a patient suffering from significant health problems and in the stratification of patient to develop better targeted treatment plans.

The proposed framework proceeds by reading a specific-organ annotated MR image volume slice by slice, after which the organ volume is calculated. The annotated organ data is processed and modelled as a volume through interpolation, polygon mesh, Gaussian smoothing and isosurface techniques, followed by a coating of Laplacian smoothing. It is useful to note that in medical imaging, isosurfaces are

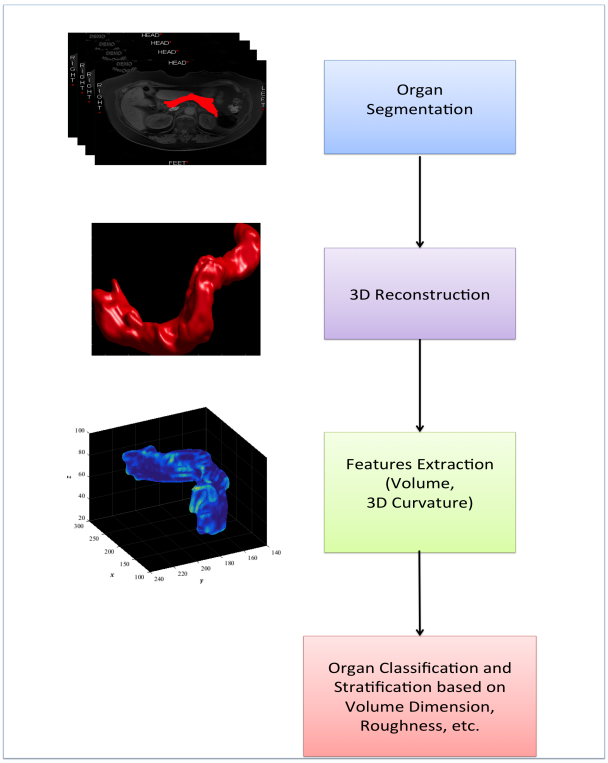

Figure 1. Overview of the steps involved in the proposed framework. The organ is segmented, reconstructed and analysed in order to extract, classify and stratify morphological information.

readily used to represent regions of a particular density in a 3D image scan, allowing the visualisation of internal organs and other structures [10]. Afterwards, the 3D curvature of the organ is calculated on a triangular mesh.

In Section II, the methodology for organ reconstruction, and volume and curvature computation are explained. Section III presents and discusses the results' outcome, comparing a set of volume and curvature calculations. Section IV provides a conclusion for the proposed framework including reference to probable future work in the area of morphological feature-based organ classification.

II. Methodology

The proposed framework consists of different steps. A set of slices from a MR image volume have to be analysed and manually annotated in order to reconstruct the 3D mesh of the organ of interest. Following an accurate 3D reconstruction, it will be possible to extract important features related to the shape, surface and dimension of the organ. These features represent important imaging biomarkers, which can be utilised for further classification and study of the organ. A schematic representation of the process is provided in Figure 1.

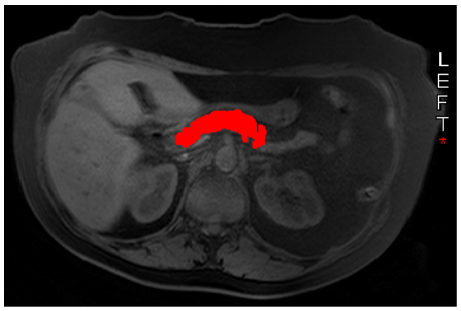

Figure 2. Manual identification of the pancreas region in one slice from a MRI volume.

A. Contouring of the Organ

Initially, an expert operator manually contours the organ of interest from the MR image volumes. Using a medical image analysis tool, the operator can process the MR image slice by slice, and identify in each slice the region where the organ is visible and identifiable. Figure 2 displays an example of a manual segmentation of the pancreas in a MR image. However, the manual segmentation of the organ represents the main bottleneck in our tool since it is a very time-consuming and operator-dependent task. In future, it is possible to replace this step by a program that automatically extracts the contour of the organ of interest from MR image volumes.

B. Reconstructing the Organ

A 3D binary volume is produced from the segmented MR images. The reconstruction process employs a Gaussian smoothing algorithm that is applied to the 3D interpolated data as a means to reduce image noise. Such a smoothing technique is often used as a pre-processing stage in computer vision tasks in order to enhance image structures at varying scales of visualisation [11]. The equation of a Gaussian function in 3D is the product of three 1D Gaussian functions as described in Equation 1:

$$G(x,y,z) = \frac{1}{2\pi\sigma^2}\exp\left(-\frac{x^2+y^2+z^2}{2\sigma^2}\right) \quad (1)$$

where x is the distance from the origin in the horizontal axis, y is the distance from the origin in the vertical axis, z is the distance from the origin in the depth axis, and σ is the standard deviation of the Gaussian distribution. The values acquired from this Gaussian distribution are used to build a convolution array which is applied to the original organ data.

Having undergone Gaussian smoothing, the filtered organ data can now be represented as an isosurface. The isosurface can be described as a set of points for which the function represented by the volume data takes on a common value, that common value being an isovalue. The marching cubes algorithm [12], used for constructing the isosurface,

proceeds by taking eight neighbour locations at a time, whereby forming an imaginary cube, and then determines the polygons needed to embody the part of the isosurface that passes through this cube. Afterwards, the individual polygons are then merged into the desired surface. This is performed by creating an index to an array of 256 possible polygon configurations within the imaginary cube. Every one of the 8 scalar values is considered 1-bit in an 8-bit integer. If the value of the scalar is higher than the isovalue, then this bit is set to 1; if it is lower than the isovalue, it is set to 0. Once all 8 scalars have been examined, the final value is the actual index to the polygon indices array. Following this, each vertex of the created polygons is placed on the appropriate position along the imaginary cubes edge by performing linear interpolation on the two scalar values that are connected by that edge.

In computer graphics, Laplacian smoothing is an algorithm readily used to smooth a polygonal mesh. In this case, the mesh is a rectangular 3D grid, thus the operation produces the Laplacian of the mesh. The proceeding implementation of a Laplacian algorithm returns a smoothed array of vertices coordinates list. For each vertex in the mesh, a new position is chosen based on local information relating to the position of neighbouring vertices, and the vertex is moved in that direction. Mathematically, the smoothing operation may be described, for each vertex, in Equation 2:

$$\overline{v}_i = \frac{1}{N}\sum_{j=1}^{N}\overline{v}_j \tag{2}$$

where N is the number of adjacent vertices to node i, $\overline{v}_j$ is the position of the j-th adjacent vertex and $\overline{v}_i$ is the new position for node i.

Once the 3D reconstruction process is complete, the 3D organ model is visualised against one slice from the original non-annotated MR image volume.

C. Computing the Volume and Curvature

Initially, the total pancreas area on each slice is computed as the actual area or the respective organ annotated pixel area; the pancreas volume per section is calculated as the product of each pancreas area and the MRI section thickness.

The 3D curvature of the organ is calculated on a triangular mesh by utilising the algorithm presented in [13], which is discussed in this section as follows. The curvature of a surface intrinsically describes the local shape of that surface. Figure 3 represents $\boldsymbol{d}(x, y)$, which is a regular surface $\boldsymbol{S}$. The point $\boldsymbol{q}$ lies on the surface $\boldsymbol{S}$. The orientation of $\boldsymbol{S}$ at $\boldsymbol{q}$ is the unit length normal $\boldsymbol{N}$. A regular curve $\boldsymbol{R}$ on $\boldsymbol{S}$ is parameterised by $\beta(a) = \boldsymbol{d}(x(a), y(a))$, where a is the arc length of $\boldsymbol{R}$, and with $\beta(0) = \boldsymbol{q}$. For all curves lying on a surface $\boldsymbol{S}$ and having at a given point $\boldsymbol{q} \in \boldsymbol{S}$, the same tangent line has at this point the same normal curvatures.

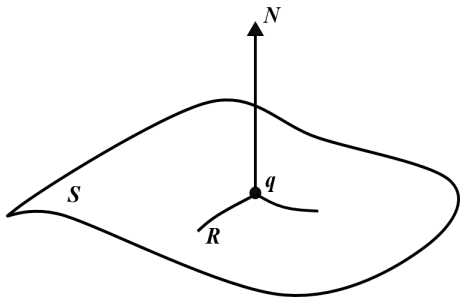

Figure 3. A point $\boldsymbol{q}$ is at a surface $\boldsymbol{S}$ with unit length normal $\boldsymbol{N}$ [12]. A regular curve $\boldsymbol{R}$ on the surface $\boldsymbol{S}$ passes through point $\boldsymbol{q}$.

This means it is possible to refer to the normal curvature along a given direction at $\boldsymbol{q}$.

If $\boldsymbol{q}_1$ with unit length surface normal $\boldsymbol{N}_1$ is another different point on the surface very close to $\boldsymbol{q}$, and $\boldsymbol{t}$ is the normalised projection of the vector $(\boldsymbol{q}_1 - \boldsymbol{q})$ onto the tangent plane at $\boldsymbol{q}$, the normal curvature, $c_n(\boldsymbol{t})$, along the tangent direction $\boldsymbol{t}$ can be approximated as described in Equation 3:

$$c_n(\boldsymbol{t}) = \frac{< \boldsymbol{q}_1 - \boldsymbol{q},\, \boldsymbol{N}_1 - \boldsymbol{N} >}{\|\boldsymbol{q}_1 - \boldsymbol{q}\|^2} \tag{3}$$

where,

$$\boldsymbol{t} = \frac{(\boldsymbol{q}_1 - \boldsymbol{q}) - < \boldsymbol{q}_1 - \boldsymbol{q},\, \boldsymbol{N} > \boldsymbol{N}}{\| (\boldsymbol{q}_1 - \boldsymbol{q}) - < \boldsymbol{q}_1 - \boldsymbol{q},\, \boldsymbol{N} > \boldsymbol{N}\|} \tag{4}$$

The next stage incorporates a triangular mesh $\boldsymbol{M} = (\boldsymbol{P}, \boldsymbol{C})$, which can be viewed as an approximation of an unknown smooth surface. If $\boldsymbol{P}$ is considered as a set of data points, then $\boldsymbol{C}$ can be described as the linking of $\boldsymbol{P}$ to construct edges and faces in $\boldsymbol{M}$. The objective is to estimate the principal curvatures and principal directions at the vertices of $\boldsymbol{M}$. The process begins by estimating the normal vectors at the vertices of the triangular mesh. The triangular face in $\boldsymbol{M}$ can be known as f. Since the triangular faces of the mesh are in the form of a plane, each of these faces f_i has a corresponding unit length normal vector $\boldsymbol{N}_{f_i}$, and the triangular mesh is positioned such that all these normal vectors are pointing to the same side of the surface. The normal at vertex $\boldsymbol{q}$ of $\boldsymbol{M}$ as a weighted average normal to the triangular faces adjacent to $\boldsymbol{q}$, is described in Equation 5:

$$N = \frac{\sum_{i=1}^{m} w_i \boldsymbol{N}_{f_i}}{\| \sum_{i=1}^{m} w_i \boldsymbol{N}_{f_i} \|} \tag{5}$$

where $\boldsymbol{N}_{f_i}$ are the unit length normal to the triangles in the "one-ring" neighbourhood of $\boldsymbol{q}$ and w_i is the weight, which is chosen based on the centre of the triangle face, f_i.

The number of points in a set of one-ring neighbour vertices of $\boldsymbol{q}$ is represented by m.

For each neighbour $\boldsymbol{q}_i$ of $\boldsymbol{q}$, $\boldsymbol{t}_i$ can be defined as the unit length projection of the vector $(\boldsymbol{q}_i - \boldsymbol{q})$ onto the tangent plane as described in Equation 6:

$$\boldsymbol{t}_i = \frac{(\boldsymbol{q}_i - \boldsymbol{q}) - < \boldsymbol{q}_i - \boldsymbol{q},\, \boldsymbol{N} > \boldsymbol{N}}{\| (\boldsymbol{q}_i - \boldsymbol{q}) - < \boldsymbol{q}_i - \boldsymbol{q},\, \boldsymbol{N} > \boldsymbol{N} \|} \quad (i = 1, ..., m) \tag{6}$$

From here, it is possible to approximate the normal curvature $c_n(\boldsymbol{t}_i)$ using Equation 3, such that:

$$c_n(\boldsymbol{t}_i) = -\frac{< \boldsymbol{q}_i - \boldsymbol{q},\, \boldsymbol{N}_i - \boldsymbol{N} >}{< \boldsymbol{q}_i - \boldsymbol{q},\, \boldsymbol{q}_i - \boldsymbol{q} >} \quad (i = 1, ..., m) \tag{7}$$

Thus, the curvature of the organ is calculated on a triangular mesh and it is based on local neighbourhood elements and vertices. It should be noted, however, that at vertices with few adjacent triangles, (and, thus, few adjacent vertices) are expanded to a greater neighbourhood. The size of the neighbourhood can heavily affect results, therefore increasing the neighbourhood size provides less sensitivity to noise [14], whereas a smaller neighbourhood size provides better curvature estimates for less noisy data.

In order to estimate the roughness and smoothness of the organ surface, a global curvature C_g has been computed as the mean value of the j local curvatures as follows:

$$C_g = \frac{1}{N} \sum_{j=1}^{N} \boldsymbol{c_j} \tag{8}$$

Organs with a global curvature higher than a threshold are considered to have a rough surface. Vice versa, organs with a global curvature less than a threshold represent a smooth surface.

III. Experiments and Discussion

The manual annotation of organs of interest such as the liver, pancreas and kidneys for MRI volumes, each of size $384 \times 384 \times 50$, were provided for experimental purposes. An experienced operator analysed and manually annotated T2 weighted MR images from 115 subjects from our database of volunteers. In particular the pancreas region has been manually segmented using a commercially available image analysis software (SliceOmatic by Tomovision). The manually annotated contours, superimposed on the MR images (Figure 2), are then extracted and elaborated by our software. A 3D binary volume is generated and processed in order to provide a final 3D approximation of the surface using the techniques described in Sections I and II. In order to calculate the curvature, a number of 50 neighbouring points have been chosen.

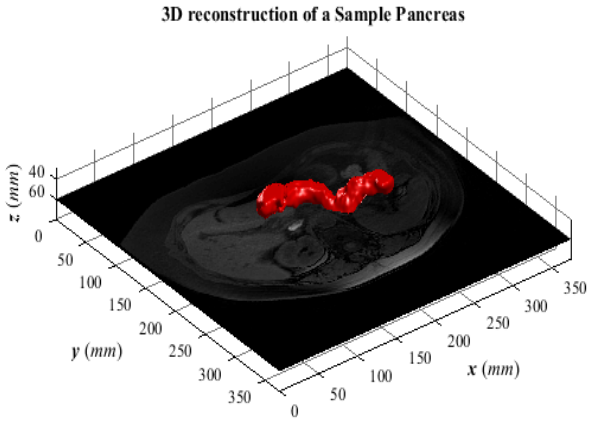

Figure 4. A 3D reconstruction of the pancreas is drawn against one slice from its corresponding MRI volume.

The results presented in this paper focus on the pancreas of 115 different adult volunteers. For each case, the volume and 3D global curvature was calculated in order to classify the pancreas in terms of volume and surface smoothness. This classification and extraction of parameters, relating to shape and texture, can be utilised to tackle fundamental clinical and scientific questions about pancreatic changes associated with the development of insulin resistance and diabetes, as well as for diagnosis and aiding image guidance systems.

Figure 4 displays a typical 3D model of the pancreas reconstructed from one of the volunteers. The 3D reconstruction presented in Figure 5 shows the depth of the pancreas curvature highlighted by varying shades of yellow. From 115 different samples, we found a wide variation in organ size. The overall mean volume was $64.7 \pm 18.4\ cm^3$ and the 3D global curvature was 0.0464 ± 0.0391. Differences in pancreas volume has been reported in literature and they may be associated with age, gender and health status of the participants [15]. A statistical representation of the data is provided in Figure 6.

As highlighted in Figure 7, the pancreas volume in relation to the curvature displays a slight weak, but significant, negative correlation. Indeed, the volume and the global curvature of the pancreas, when compared using a Wilcoxon signed-rank test, showed a statistically significance difference ($p < 0.0001$), and using a t-test ($p < 0.0001$).

If we consider the morphology of the pancreas being described by the global curvature of the organ shape, then based on our results, we can expect that as the size of the organ decreases, higher values of global curvature are anticipated, thus increasing the irregularities in the shape. Indeed, changes in volume size and morphology have been

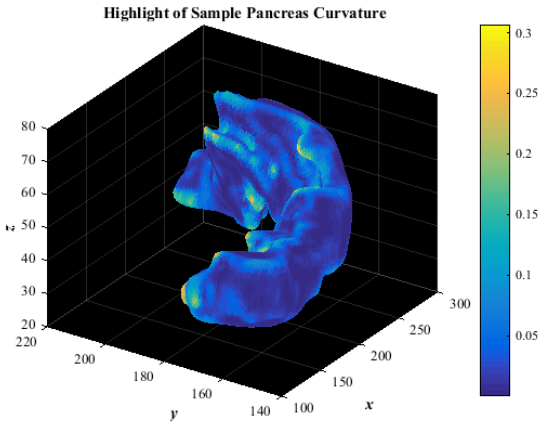

Figure 5. The depth of a pancreas curvature is highlighted by varying shades of yellow.

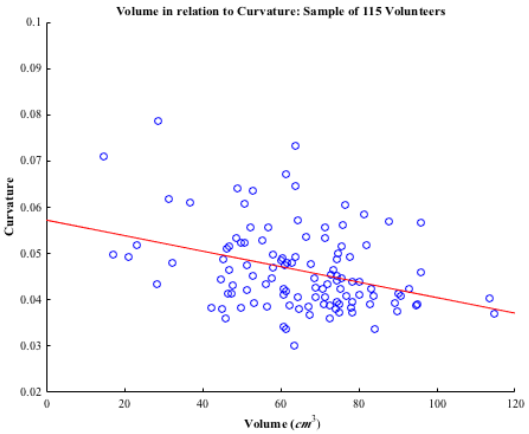

Figure 7. The pancreas volume in relation to the curvature displays a slight negative correlation.

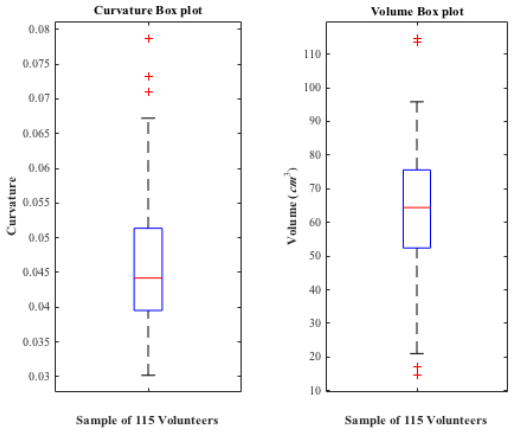

Figure 6. Box plot for 3D curvature and volume of 115 cases.

previously observed in some subjects with type 2 diabetes, where the pancreas displayed an involuted morphology with serrated borders [16]. Given the increase in global incidences of type 2 diabetes and the broad clinical spectrum of the disease, there is a clear need for a better understanding of the relationship between morphology and function in order to provide insightful stratification of patients and objective measurements of disease progression, and remission, especially where changes in organ morphology have been observed but not quantified. This clearly demands objective and reliable methodologies to obtain more in-depth morphological characterization of the pancreas and associated organs.

Furthermore, the framework presented here can be used in large cohort studies; for example, the UK BioBank provides details of an estimated 100,000 subjects who will undergo phenotyping, including a full body MRI. Such studies will serve as the basis for stratifying patients with type 2 diabetes as well as been extended to ascertain correlation between morphological changes of a given organ to other relevant information from the participants, including genetic and life-style factors.

As concerns the computational complexity of the proposed method, in terms of classification based on volume and surface smoothness, it is low because the proposed method only evaluates two formulas, one for the calculation of the volume and the other for the global curvature of the 3D reconstructed organ. The proposed method, compared with other machine learning techniques that could be used for classification purposes, does not require a pre-training stage, thus there is no need to manually label a high number of 3D reconstructed organs.

IV. Conclusion

Driven by the knowledge in which accurate 3D organ reconstruction, coupled with size and structure analysis, can support medical professionals in their clinical diagnosis, detection and planning of treatment, this paper describes a computing tool that classifies organs based on factors such as volume and curvature using anonymised volunteer data from magnetic resonance (MR) image volumes. In addition to offering radiologists a “second opinion” upon inspection, thus helping to eliminate possible misdiagnosis, tools such as this can be easily used in the scope of much greater research and investigation including forensic science and biomedicine; it can also be incorporated into the development of effective medical image analysis software applications. In future work, this tool could extend towards the automatic classification of variations in an organ based on volume, curvature and other factors such as age, gender, weight and height. This would assume no operator involvement other than providing the relevant MRI patient scan. The automatic classification algorithm would be able to accurately segment the desired organ from the given

image and perform analysis in order to detect possible abnormalities or features linked with a particular disorder.

ACKNOWLEDGMENT

The authors would like to thank the University of Westminster for providing a large medical imaging dataset that fosters research for health and wellbeing. The authors are also grateful to Grogoire Gesmier and the Centre of Parallel Computing at University of Westminster for supporting the deployment of the experiments in a parallel computing cloud.

REFERENCES

[1] N. Burute, R. Nisenbaum, D. J. Jenkins, A. Mirrahimi, S. Anthwal, E. Colak, and A. Kirpalani, "Pancreas volume measurement in patients with Type 2 diabetes using magnetic resonance imaging-based planimetry," *Pancreatology*, vol. 14, no. 4, pp. 268–274, 2014.

[2] W. R. Cnossen and J. P. Drenth, "Polycystic liver disease: an overview of pathogenesis, clinical manifestations and management," *Orphanet Journal of Rare Diseases*, vol. 9, no. 1, p. 69, 2014. [Online]. Available: http://dx.doi.org/10.1186/1750-1172-9-69

[3] E. M. Geraghty, J. M. Boone, J. P. McGahan, and K. Jain, "Normal organ volume assessment from abdominal CT," *Abdominal Imaging*, vol. 29, no. 4, pp. 482–490, 2004. [Online]. Available: http://dx.doi.org/10.1007/s00261-003-0139-2

[4] L. B. Uittenbogaard, M. C. Haak, R. J. H. Peters, G. M. van Couwelaar, and J. M. G. Van Vugt, "Validation of volume measurements for fetal echocardiography using four-dimensional ultrasound imaging and spatiotemporal image correlation," *Ultrasound in Obstetrics and Gynecology*, vol. 35, no. 3, pp. 324–331, 2010. [Online]. Available: http://dx.doi.org/10.1002/uog.7561

[5] J. R. Meakin, J. Fulford, R. Seymour, J. R. Welsman, and K. M. Knapp, "The relationship between sagittal curvature and extensor muscle volume in the lumbar spine," *Journal of Anatomy*, vol. 222, no. 6, pp. 608–614, 2013. [Online]. Available: http://dx.doi.org/10.1111/joa.12047

[6] Z. Li, D. Zou, J. Zhang, Y. Shao, P. Huang, and Y. Chen, "Use of 3D reconstruction of emergency and postoperative craniocerebral CT images to explore craniocerebral trauma mechanism," *Forensic Science International*, vol. 255, pp. 106–111, 2015, international Association of Forensic Sciences (IAFS) 20th Meeting.

[7] J. Van de Velde, S. Bogaert, P. Vandemaele, W. Huysse, E. Achten, J. Leijnse, W. De Neve, and T. Van Hoof, "Brachial plexus 3D reconstruction from mri with dissection validation: a baseline study for clinical applications," *Surgical and Radiologic Anatomy*, vol. 38, no. 2, pp. 229–236, 2016. [Online]. Available: http://dx.doi.org/10.1007/s00276-015-1549-x

[8] Y. Zhang, Y. Zhou, X. Yang, P. Tang, Q. Qiu, Y. Liang, and J. Jiang, "Thin slice three dimentional (3D) reconstruction versus CT 3D reconstruction of human breast cancer," *Indian Journal of Medical Research*, vol. 137, no. 1, pp. 57–62, 2013.

[9] K.-M. Lee, J.-M. Song, J.-H. Cho, and H.-S. Hwang, "Influence of head motion on the accuracy of 3D reconstruction with cone-beam CT: Landmark identification errors in maxillofacial surface model," *PLOS ONE*, vol. 11, no. 4, pp. 1–10, April 2016. [Online]. Available: https://doi.org/10.1371/journal.pone.0153210

[10] C. Wang and S. Lai, *Adaptive Isosurface Reconstruction Using a Volumetric-Divergence-Based Metric*. Cham: Springer International Publishing, 2016, pp. 367–378.

[11] A. M. Wink and J. B. T. M. Roerdink, "Denoising functional MR images: a comparison of wavelet denoising and Gaussian smoothing," *IEEE Transactions on Medical Imaging*, vol. 23, no. 3, pp. 374–387, March 2004.

[12] C.-s. Dong and G.-z. Wang, "Curvatures estimation on triangular mesh," *Journal of Zhejiang University-SCIENCE A*, vol. 6, no. 1, pp. 128–136, 2005. [Online]. Available: http://dx.doi.org/10.1007/BF02887228

[13] W. E. Lorensen and H. E. Cline, "Marching Cubes: A High Resolution 3D Surface Construction Algorithm," *SIGGRAPH Comput. Graph.*, vol. 21, no. 4, pp. 163–169, 1987. [Online]. Available: http://doi.acm.org/10.1145/37402.37422

[14] S. Rusinkiewicz, "Estimating curvatures and their derivatives on triangle meshes," in *Symposium on 3D Data Processing, Visualization, and Transmission*, September 2004.

[15] V. Caglar, B. Kumral, R. Uygur, O. Alkoc, O. Ozen, and D. H., "Study of volume, weight and size of normal pancreas, spleen and kidney in adults autopsies," *Forensic Medicine and Anatomy Research.*, vol. 2, no. 3, pp. 63–69, 2014.

[16] M. Macauley, K. Percival, P. E. Thelwall, K. G. Hollingsworth, and R. Taylor, "Altered Volume, Morphology and Composition of the Pancreas in Type 2 Diabetes," *PLOS ONE*, vol. 10, no. 5, pp. 1–14, May 2015. [Online]. Available: https://doi.org/10.1371/journal.pone.0126825